International Journal of Rotating Machinery, 9(1): 11–22, 2003

1023-621X/03 $12.00 + .00
DOI: 10.1080/10236210390147317

Taylor & Francis
Taylor & Francis Group

# Advances in Unsteady Boundary Layer Transition Research, Part II: Experimental Verification

**M. T. Schobeiri and L. Wright**
*Turbomachinery Performance and Flow Research Laboratory, Department of Mechanical Engineering, Texas A&M University, College Station, Texas, USA*

**This two-part article presents recent advances in boundary layer research into the unsteady boundary layer transition modeling and its validation. This, Part II, deals with the results of an inductive approach based on comprehensive experimental and theoretical studies of unsteady wake flow and unsteady boundary layer flow. The experiments were performed on a curved plate at a zero streamwise pressure gradient under periodic unsteady wake flow, in which the frequency of the periodic unsteady flow was varied. To validate the model, systematic experimental investigations were performed on the suction and pressure surfaces of turbine blades integrated into a high-subsonic cascade test facility, which was designed for unsteady boundary layer investigations. The analysis of the experiment's results and comparison with the model's prediction confirm the validity of the model and its ability to predict accurately the unsteady boundary layer transition.**

**Keywords** boundary, layer, transition, unsteady

Analysis of the experimental data derived from the curved plate (discussed in Part I) resulted in the unsteady intermittency function $\Gamma$, shown in Figures 1a and 1b, for frequency values of $\Omega = 1.033$ (three rods) and 3.443 (ten rods), respectively, with the dimensionless longitudinal distance $s/s_0$ as a parameter. Similar results were observed for other rod frequencies (see Table 1 in Part I). The symbols represent the experimental data. For the reduced frequencies and longitudinal positions presented in these plots, the measured relative intermittency functions for wakes impinging on the plate surface closely follow a Gaussian distribution, which is given by

$$\Gamma = e^{-\zeta^2} \qquad [1]$$

Here, $\zeta$ is the nondimensionalized lateral length scale defined in Part I. The function $\Gamma$ is an unsteady intermittency relationship that is also valid for various pressure gradients. The intermittency function $\langle\gamma_i(t_i)\rangle$ is completely determined if additional information about the minimum and maximum intermittency functions, $\langle\gamma_i(t_i)\rangle_{\min}$ and $\langle\gamma_i(t_i)\rangle_{\max}$, is available. The distribution of $\langle\gamma_i(t_i)\rangle_{\min}$ and $\langle\gamma_i(t_i)\rangle_{\max}$ in the streamwise direction is plotted in Figure 2 for $\Omega = 1.033$ (three rods). The steady case (no rods) shown in Figure 3 serves as the basis for comparison of these minimum and maximum values. In the steady case, the intermittency rises from zero at a streamwise Reynolds number, $\mathrm{Re}_{x,s} = 2 \times 10^5$, and gradually approaches the unity corresponding to the fully turbulent state. This is typical of natural transition and follows the intermittency function introduced by Narasimha (1957). The distributions of minimum and maximum turbulence intermittencies, $\langle\gamma_i(t_i)\rangle_{\min}$ and $\langle\gamma_i(t_i)\rangle_{\max}$, in the streamwise direction are shown in Figure 2. For each particular streamwise location on the plate surface with a streamwise Reynolds number, for example $\mathrm{Re}_{x,s} = 1 \times 10^5$, two corresponding, distinctively different intermittency states are periodically present. At this location, $\langle\gamma_i(t_i)\rangle_{\max}$ corresponds to the condition when the wake with the high turbulence intensity core impinges on the plate surface at a particular instant of time. Once the wake has passed over the surface, the same streamwise location is exposed to a low turbulence intensity flow regime with an intermittency state of $\langle\gamma_i(t_i)\rangle_{\min}$, where no wake is present. As may be seen, $\langle\gamma_i(t_i)\rangle_{\min}$ has the tendency to follow the course of the steady (no wake) intermittency distribution exhibited in Figure 3, with a gradual increase from an initial nonturbulent state that has a value of zero and approaching a final state of 0.8. This was expected, as $\langle\gamma_i(t_i)\rangle_{\min}$ is calculated outside the wake region, where the turbulence intensity is relatively small. On the other hand, $\langle\gamma_i(t_i)\rangle_{\max}$ reveals a fundamentally different behavior that needs to be discussed further. As Figure 2 shows, the wake flow

Received 28 March 2001; accepted 12 April 2001.
Address correspondence to M. T. Schobeiri, Turbomachinery Performance and Flow Research Laboratory, Department of Mechanical Engineering, Texas A&M University, College Station, TX 77843-3123, USA. E-mail: tschobeiri@mengr.tamu.edu

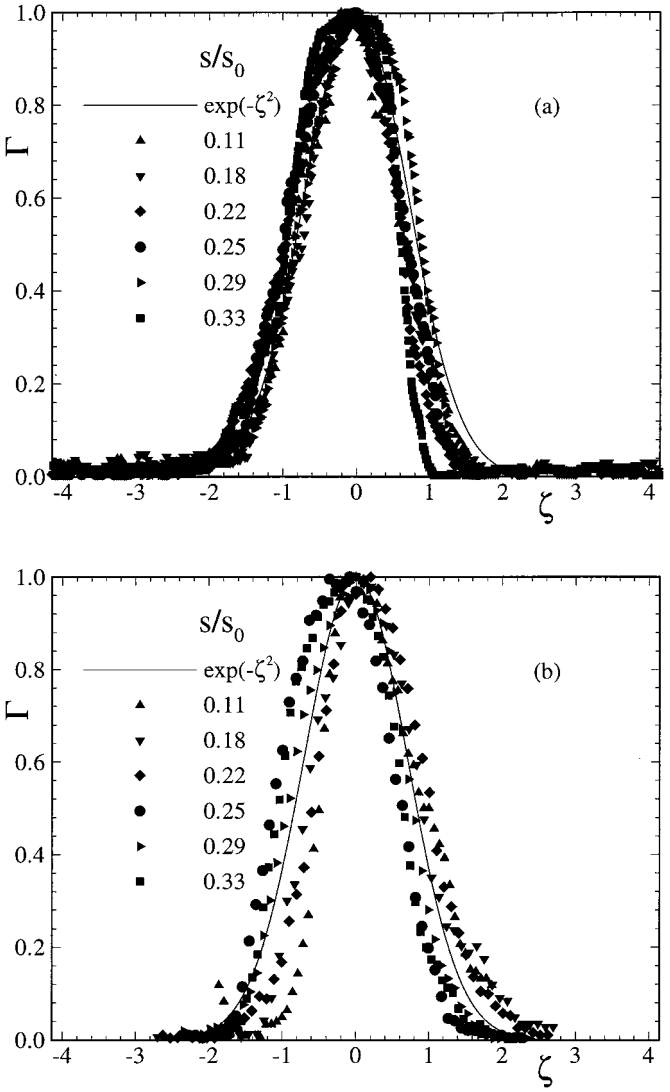


**FIGURE 1**
Relative intermittency as a function of nondimensionalized lateral coordinates. (a) $\Omega = 1.033$ (3 rods). (b) $\Omega = 3.443$ (10 rods) on the curved plate.

with an intermittency close to 1 impinges on the blade surface. By convecting downstream, its turbulent fluctuations undergo a strong damping by the wall's shear stress forces. The process of damping continues until $<\gamma_i(t_i)\rangle_{\max}$ reaches a minimum. At that point, the wall's shear forces are not able to further suppress the turbulent fluctuations. As a consequence, the intermittency again increases and approaches the unity, showing the combined effect of wake-induced and natural transition because of an increased level of turbulence intensity. The damping process of the high-turbulence intensity wake flow discussed above explains the phenomenon of the becalming effect of a wake-induced transition observed by several researchers, including Pfeil and Herbst (1979) and Schobeiri et al. (1995). Figure 2 also shows the average intermittency, which is a result of the

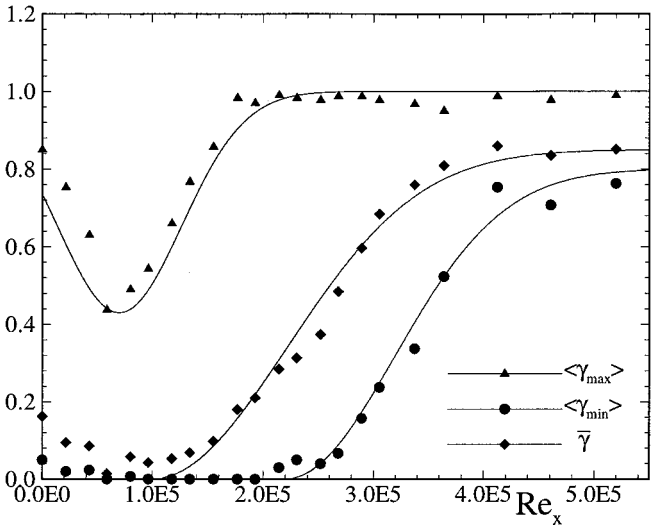


**FIGURE 2**
Maximum, minimum, and time-averaged intermittency distributions as a function of the axial Reynolds number for $\Omega = 1.033$ (3 rods).

integral effect of periodic wakes with respect to time. The maximum intermittency is described by

$$\langle\gamma(t)\rangle_{\max} = 1.0 - c_1 e^{-\left(\frac{\mathrm{Re}_x - \mathrm{Re}_{x,s}}{\mathrm{Re}_{x,s} - \mathrm{Re}_{x,e}}\right)^2} \qquad [2]$$

where the constant $c_1$ depends on $\Omega$. The minimum intermittency is described by

$$\langle\gamma(t)\rangle_{\min} = c_2\left(1.0 - e^{-\left(\frac{\mathrm{Re}_x - \mathrm{Re}_{x,s}}{\mathrm{Re}_{x,s} - \mathrm{Re}_{x,e}}\right)^2}\right) \qquad [3]$$

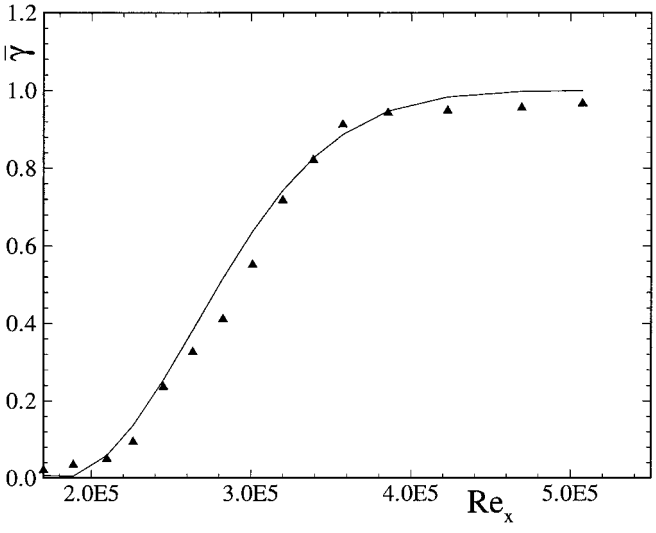


**FIGURE 3**
Intermittency as a function of $\mathrm{Re}_x$ (no rods, or steady) on the concave surface of the curved plate.

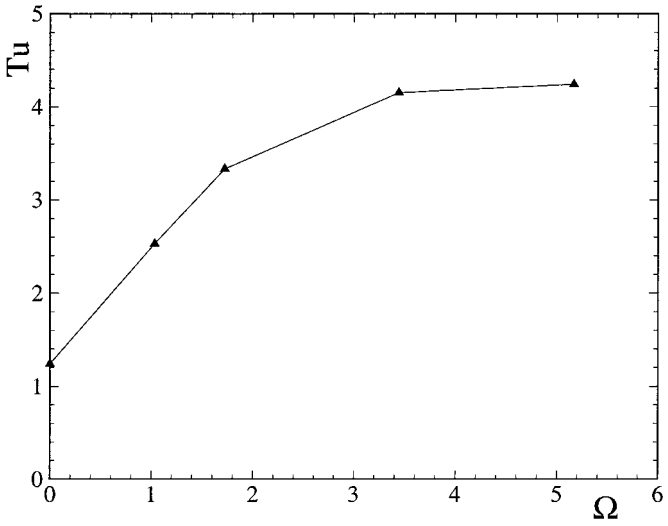


**FIGURE 4**
Time-averaged inlet freestream turbulence intensity as a function of Ω.

where the constants $c_2$ are again dependent on Ω. The time-averaged intermittency is described by

$$\overline{\gamma} = c_4\left(1.0 - c_3 e^{-\left(\frac{\mathrm{Re}-\mathrm{Re}_{x,s}}{\mathrm{Re}_{x,s}-\mathrm{Re}_{x,e}}\right)^2}\right) \qquad [4]$$

The combined effects of $\langle\gamma_i(t_i)\rangle_{\max}$ and $\langle\gamma_i(t_i)\rangle_{\min}$ can be seen in the expression for $\overline{\gamma}$ through the constants $c_3$ and $c_4$. The four constants for the frequencies under investigation are given in Table 1, Part I. For natural transition, the above constants approach unity.

One major parameter affecting the onset of the boundary layer transition is the freestream turbulence intensity. The presence of the wakes, particularly their spacing and interaction, contributes significantly to an increase in the freestream turbulence. Figure 4 shows the freestream time-averaged turbulence intensity distribution as a function of the inlet wake frequency. The reduced frequency range investigated was observed to approach a maximum value of 4.2% as the wake frequency was increased.

## CURVED-PLATE AERODYNAMIC STUDIES

### Results

*Experimental Results: Turbulence Intermittency Distribution*

The entire set of ensemble-averaged data was utilized to generate the temporal-spatial distribution of the ensemble-averaged turbulence intermittency. Figure 5 shows a representative example at $y = 0.5$ mm. As shown, the boundary layer is periodically disturbed by the wakes that cause periodically high turbulence strips and extended becalmed regions. As discussed previously, these extended becalmed regions were produced by the strong damping of turbulence fluctuations in the wall region, which led to an exponential decrease in the maximum intermittency, $\langle\gamma_i(t_i)\rangle_{\max}$. These regions were observed between the leading edge and the streamwise position of $s/s_0$ greater than 0.4. As may be seen, the wake strips are separated from the becalmed regions, indicating the absence of any visible interaction. Increasing the

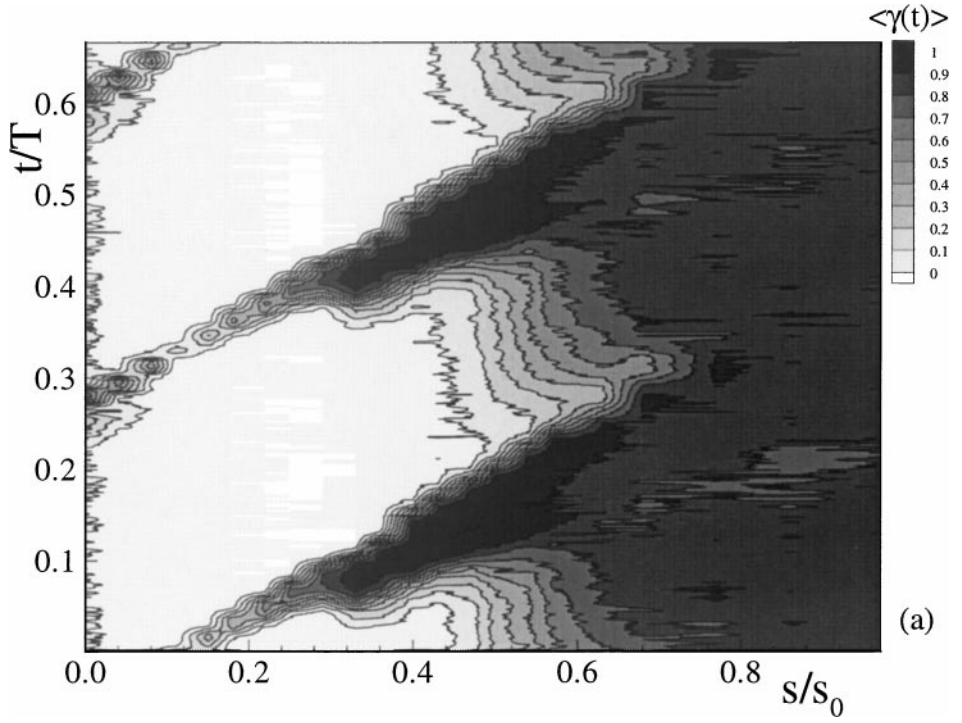


**FIGURE 5**
A contour plot of the intermittency factor as a function of the normalized axial distance, $s/s_0$, for $\Omega = 1.033$ (3 rods).

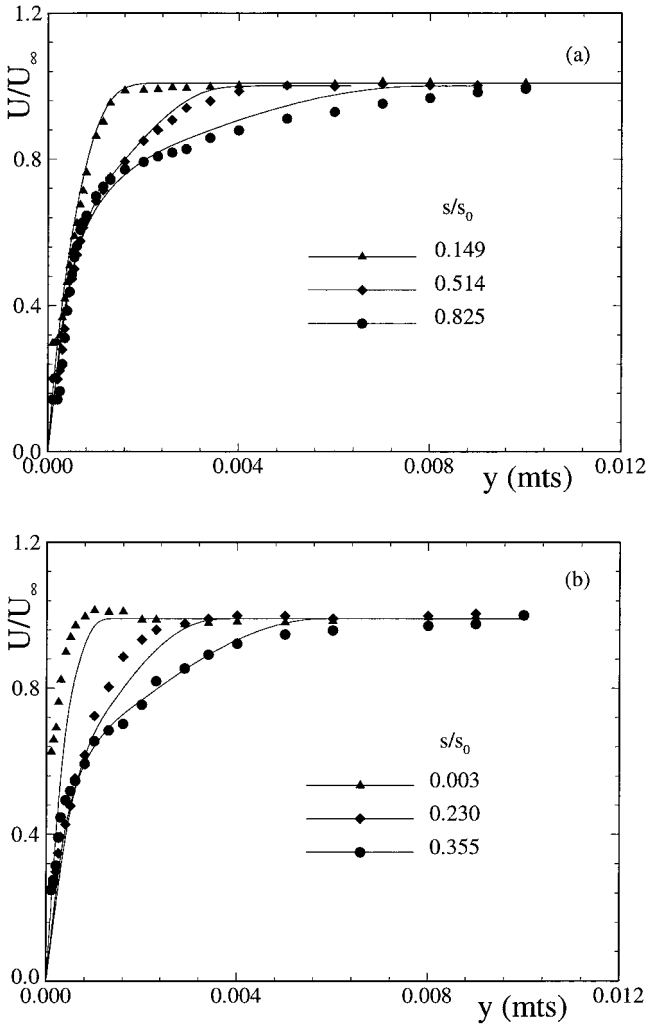


**FIGURE 6**
Velocity profiles as a function of the lateral coordinates of three axial locations. (a) $\Omega = 0.0$ (no rods). (b) $\Omega = 1.725$ (5 rods).

frequency Ω of the wake by reducing the rod spacing results in an earlier start of transition compared to the three-rod case. Two mechanisms are considered instrumental in affecting this transition start. The first is an earlier mixing of the wakes due to the reduction of their spacing, which leads to higher freestream turbulence that inherently affects the onset of the transition. The second mechanism is the increased impinging frequency of the primary wake strips, which introduces an excessive transport of turbulent kinetic energy into the boundary layer, causing the transition start to shift toward the leading edge. It is conceivable that the combination of these two mechanisms would make additional contributions to the shift of the transition start. A further increase of Ω results in greater freestream turbulence and increased impinging frequency and, thus, a significant shift of the transition toward the leading edge as the consequence of the mechanisms discussed above. A similar turbulence intermittency pattern is observed for other *y* positions.

*Calculation Results: Velocity Distributions*

Implementing the intermittency model into the calculation procedure allows the prediction of time-averaged velocity distribution. As representative examples, the time-averaged velocity profiles for $\Omega = 0$ and $\Omega = 1.725$ are plotted in Figures 6a and 6b for laminar, transitional, and turbulent flow regions. The solid lines exhibit the calculation results, which are in close agreement with the experimental results, which are represented by symbols.

## Discussion

*Heat Transfer: Steady Inlet Flow Reference Case*

Heat transfer measurement using the liquid crystal technique developed by Hippensteele and colleagues (1981) is being applied by numerous researchers. It has the advantage of not affecting the turbulence structure at the surface as thermocouples or surface-mounted hot wire/film probes do. However, its slow response does not allow the extraction of valuable information concerning unsteadiness. As a result, only time-averaged responses can be acquired in unsteady cases. This technique was used first for comparison purposes; the results of the steady-state case $\Omega = 0$ (no rod) are presented in Figure 7. Good agreement between the calculation and the experiment is shown for a wide range of $Re_x$ from the leading edge, via the transition portion, to the trailing edge. For comparison purposes, it may be noted that the model by Mayle (1991) shows a slight difference between the experiment and the theory. However, it should be pointed out that Mayle's correlation gives reasonably good results for the time-averaged unsteady cases.

*Heat Transfer: Unsteady Inlet Flow Cases*

In cases of unsteady flow with the reduced frequency values of $\Omega = 1.033$ and $\Omega = 5.166$ (see Table 1, Part I), calculated Stanton numbers were compared with the experimental results.

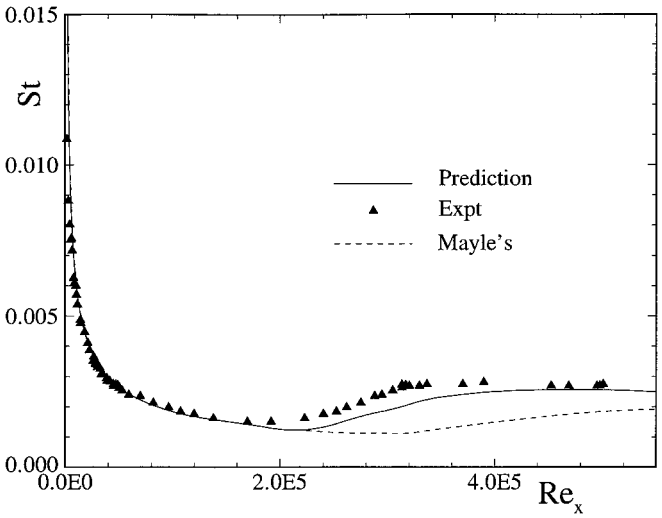


**FIGURE 7**
Stanton number as a function of the axial Reynolds number for no rods, or the steady case.

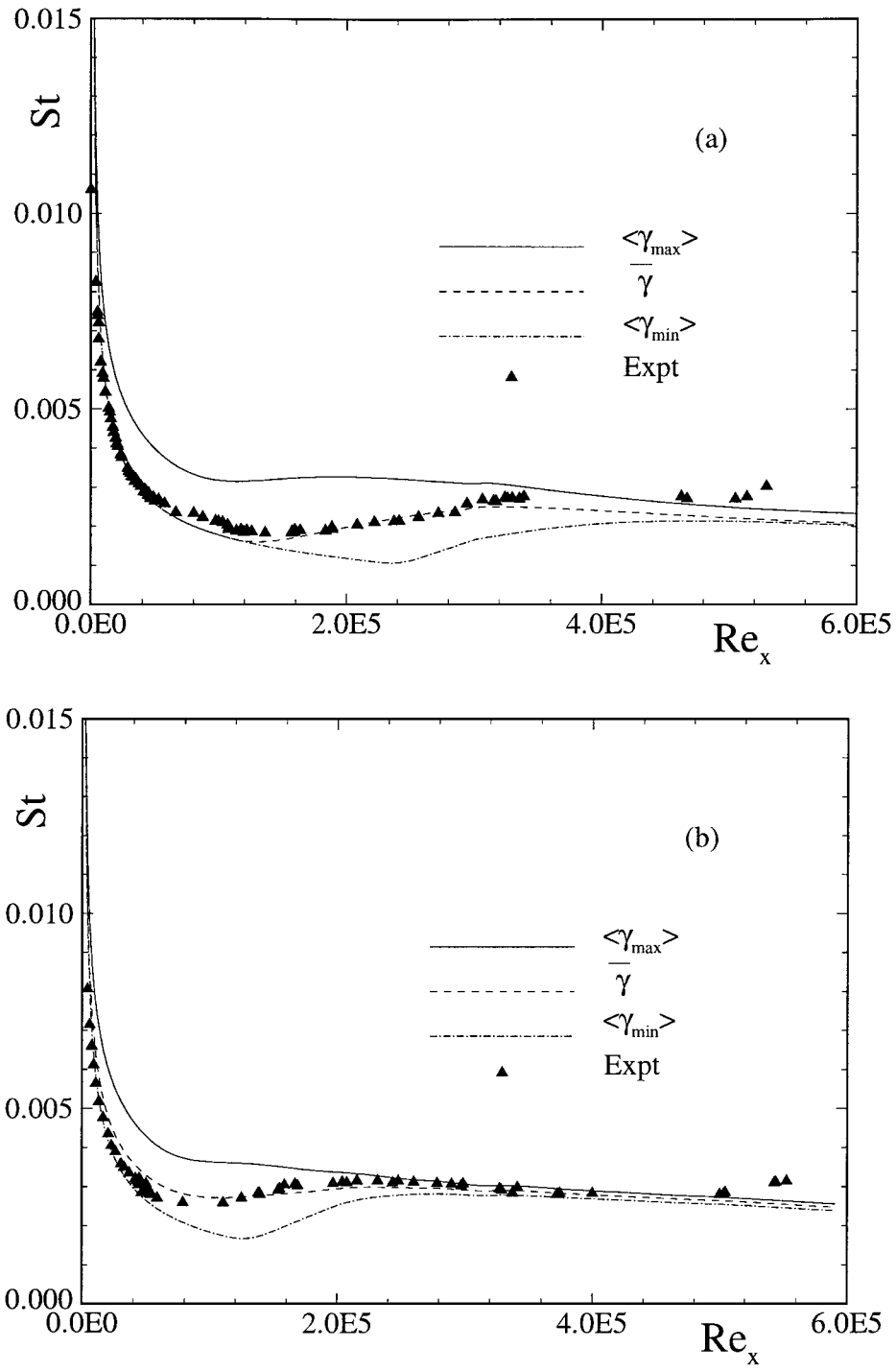


**FIGURE 8**
Stanton number as a function of the axial Reynolds number. (a) $\Omega = 1.033$ (3 rods). (b) $\Omega = 5.166$ (15 rods).

This is shown in Figures 8a and 8b, where the experimental results are represented by symbols. The three curves plotted in each diagram represent the calculation results. Starting with a reduced frequency of $\Omega = 1.033$ (3 rods), the solid line represents the distribution of the streamwise Stanton number when the plate is subjected to an inlet flow intermittency state of $\langle \gamma(t) \rangle_{\max}$. The dot-and-dash curve depicts the Stanton number distribution when the plate is subjected to $\langle \gamma(t) \rangle_{\min}$. However, because of the periodic character of the inlet flow associated with unsteady wakes, the plate would experience the periodic change of heat transfer represented by the upper and lower Stanton number curves (the solid line and the dot-and-dash line) as an envelope.

The liquid crystal responds to this periodic event with time-averaged signals. This time-averaged result is reflected by the dashed line, which gives a corresponding time-averaged intermittency. As is clear, reasonably good agreement was found for the entire laminar and transitional portions. Close to the plate's trailing edge, the theory underpredicted slightly. It should be mentioned that heat transfer measurements in this area were associated with certain difficulties.

As the experimental results show (see Figure 8b), increasing the reduced frequency to $\Omega = 5.166$ (15 rods) causes the transition point to shift toward the leading edge and results in a slightly higher Stanton number. This shift of the transition point is in full accord with the aerodynamic findings explained previously. Similar to the case in which $\Omega = 1.033$, the solid curve represents the streamwise Stanton number distribution that occurs when the plate is subjected to an inlet flow intermittency state of $\langle\gamma(t)\rangle_{\max}$. The dot-and-dash curve depicts the Stanton number distribution pertaining to the minimum intermittency, $\langle\gamma(t)\rangle_{\min}$. The time-averaged result is reflected by the dashed curve representing the streamwise Stanton number distribution that occurs when the plate is subjected to an inlet flow intermittency state of $\langle\gamma(t)\rangle_{\max}$. Figure 8b exhibits the reasonably good agreement between the theory and the experiment in the transition and turbulence regions, with $\mathrm{Re}_x$ being greater than $1.2 \times 10^5$. In the laminar region, however, the theory slightly overpredicted the heat transfer, resulting in marginally higher Stanton numbers. In this region, better agreement was reached by utilizing the minimum intermittency, $\langle\gamma(t)\rangle_{\min}$. Similar tendencies were seen for the $\Omega$ values of 1.725 (5 rods) and 3.443 (10 rods). As discussed previously, the combined effect of wake mixing and the increasing impinging frequency of the wake strips, which introduced an excessive turbulent kinetic energy transport to the boundary layer, was to cause a shift in the transition start toward the leading edge.

## UNSTEADY TURBINE CASCADE EXPERIMENTS

The relative intermittency function presented above is the result of the analysis of the boundary layer experimental data obtained from a zero-pressure gradient curved plate. In order to apply this intermittency function to turbomachinery flow cases, its validity first has to be verified. For this purpose, unsteady boundary layer experiments were performed on the unsteady turbine cascade facility described in Part I. Figure 9 shows the pressure distribution along the pressure and section surface of one of the instrumented turbine blades for both steady ($\Omega = 0.0$) and unsteady ($\Omega = 0.755$) cases. The pressure distribution showed excellent repeatability under these two conditions. The pressure signals inherently signified the time-averaged pressure because of the internal pneumatic damping effect of the pipes connecting to the transducer. The time-averaged pressure coefficient along the pressure and suction surfaces is plotted in this figure. On the suction surface (the lower portion of the plot), the flow first accelerates sharply, reaches a minimum pressure coefficient at $s/s_0 \approx 0.255$, and then continuously decelerates at a

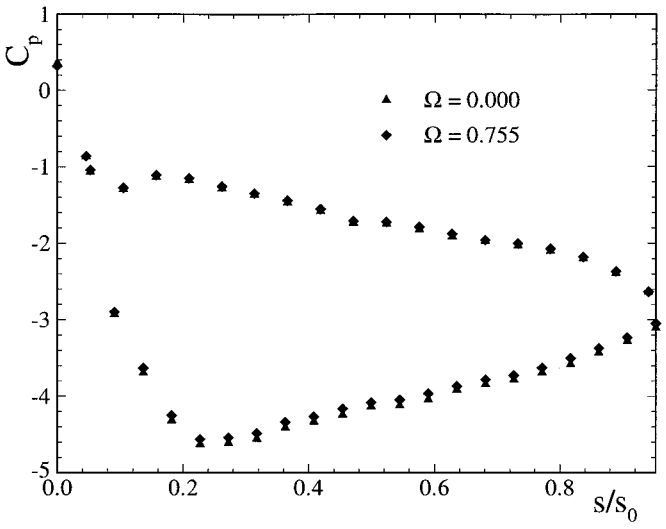


**FIGURE 9**
The static pressure distribution at $\mathrm{Re}_c = 264187$ under steady ($\Omega = 0.00$) and unsteady ($\Omega = 0.755$) flow conditions.

moderate rate until the trailing edge is reached. On the pressure surface, the flow accelerates, reaches a local minimum pressure coefficient at $s/s_0 \approx 0.1$, and is subjected to deceleration until $s/s_0 \approx 0.12$ is reached. Beyond this point, the pressure gradient on the pressure surface keeps accelerating, while on the suction surface, the decelerating pressure gradient prevails. This pressure gradient situation has a significant effect on the boundary layer development, as is discussed later. A closer look at the wake propagation is shown in Figure 10; for the wake-passing frequency $\Omega = 0.755$ at a lateral distance of $y = 2.5$ mm above the plate surface. The velocity is normalized with respect to the velocity of the corresponding steady case ($\Omega = 0$) at $y = 2.5$ mm. For the first half of the profile length on the

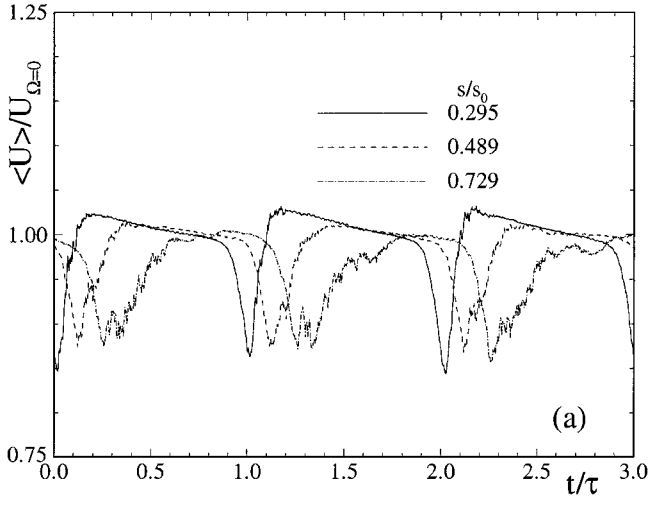


**FIGURE 10**
The ensemble-averaged velocity on the pressure surface at $y = 2.5$ mm for $\Omega = 0.755$.

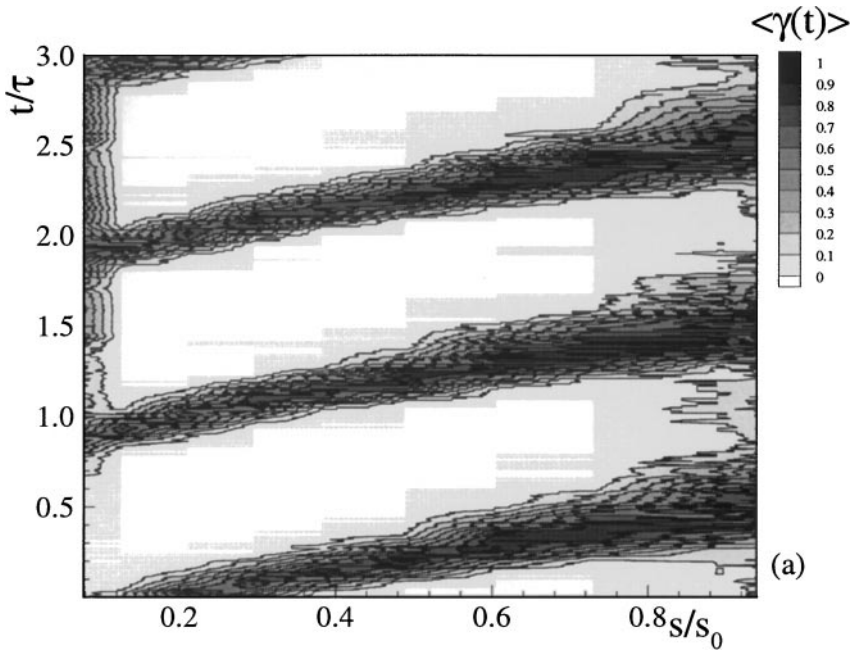


**FIGURE 11**
The ensemble-averaged intermittency factor as a function of the nondimensional distance, $s/s_0$, for $\Omega = 0.755$ on the pressure surface.

pressure surface ($s/s_0 = 0.295$ and 0.489) the velocity distributions in Figure 10 exhibit an asymmetrical behavior, indicating the effect of a strong curvature of the blade passage. This figure also shows the growth of the wake as it convects downstream.

### Intermittency Distribution

The entire set of ensemble-averaged data was utilized to generate the temporal-spatial distribution of the ensemble-averaged turbulence intermittency. Figures 11 and 12 show a representative example at $y = 0.1$ mm for $\Omega = 0.755$ and $\Omega = 1.51$. As

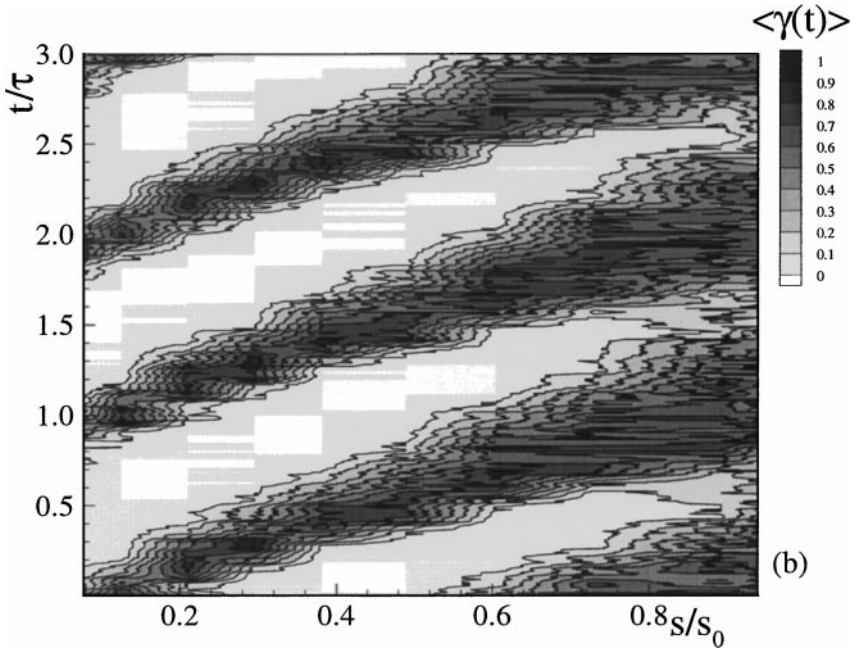


**FIGURE 12**
The ensemble-averaged intermittency factor as a function of the nondimensional distance, $s/s_0$, at $y = 0.1$ mm for $\Omega = 1.51$ on the pressure surface of the turbine blade.

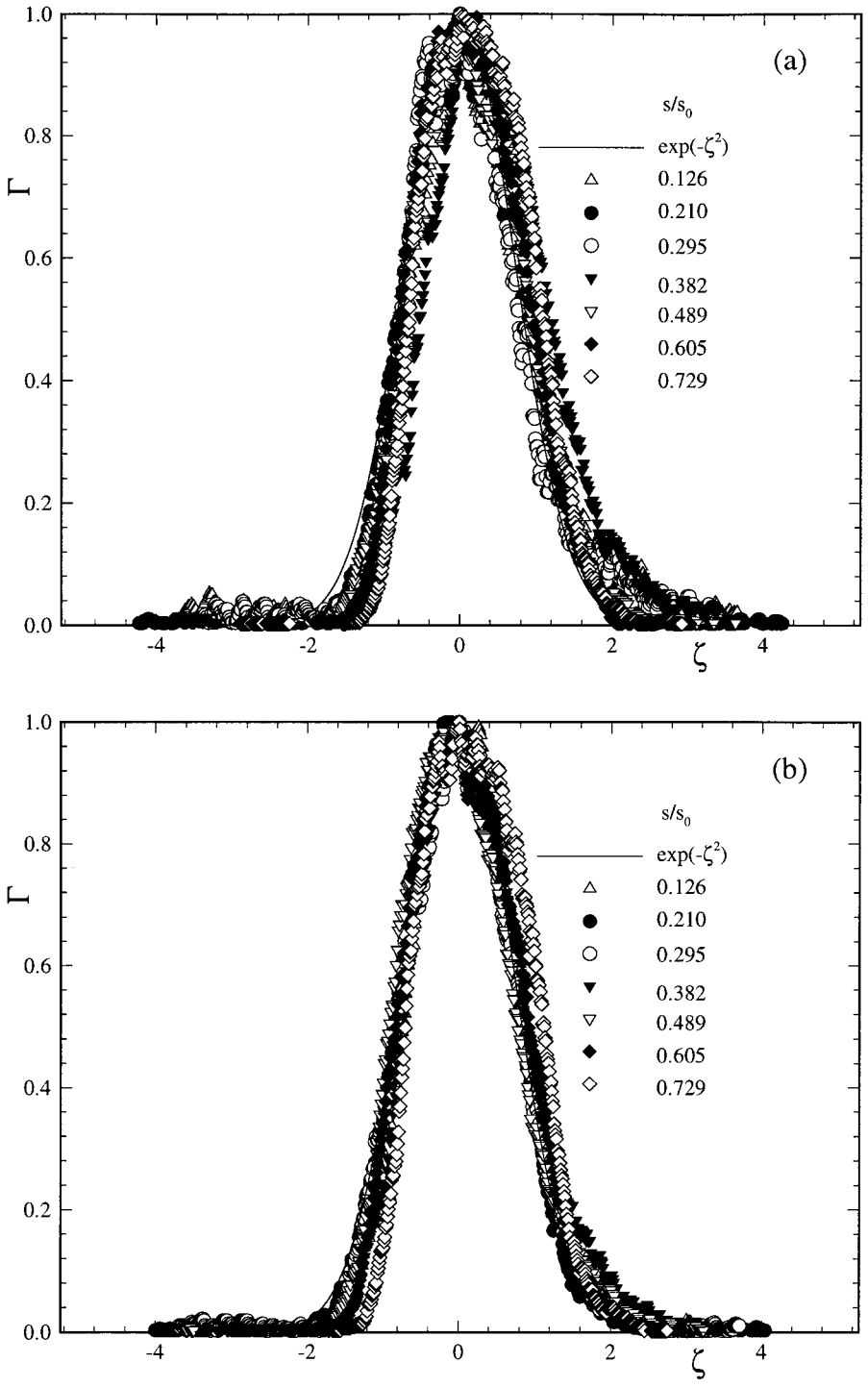


**FIGURE 13**
The relative intermittency as a function of nondimensionalized lateral coordinates. (a) $\Omega = 0.755$. (b) $\Omega = 1.51$ at $y = 0.1$ mm on the pressure surface.

shown in Figure 11, for the pressure surface ($\Omega = 0.755$, 160 mm spacing), the boundary layer was periodically disturbed by the wakes that periodically produced high-turbulence strips and extended becalmed regions. These extended becalmed regions were produced by the strong damping of turbulence fluctuations in the wall region, which resulted in an exponential decrease in the maximum intermittency, $\langle \gamma_i(t_i) \rangle_{\max}$. A similar intermittency pattern was observed on the suction surface. However, the transition

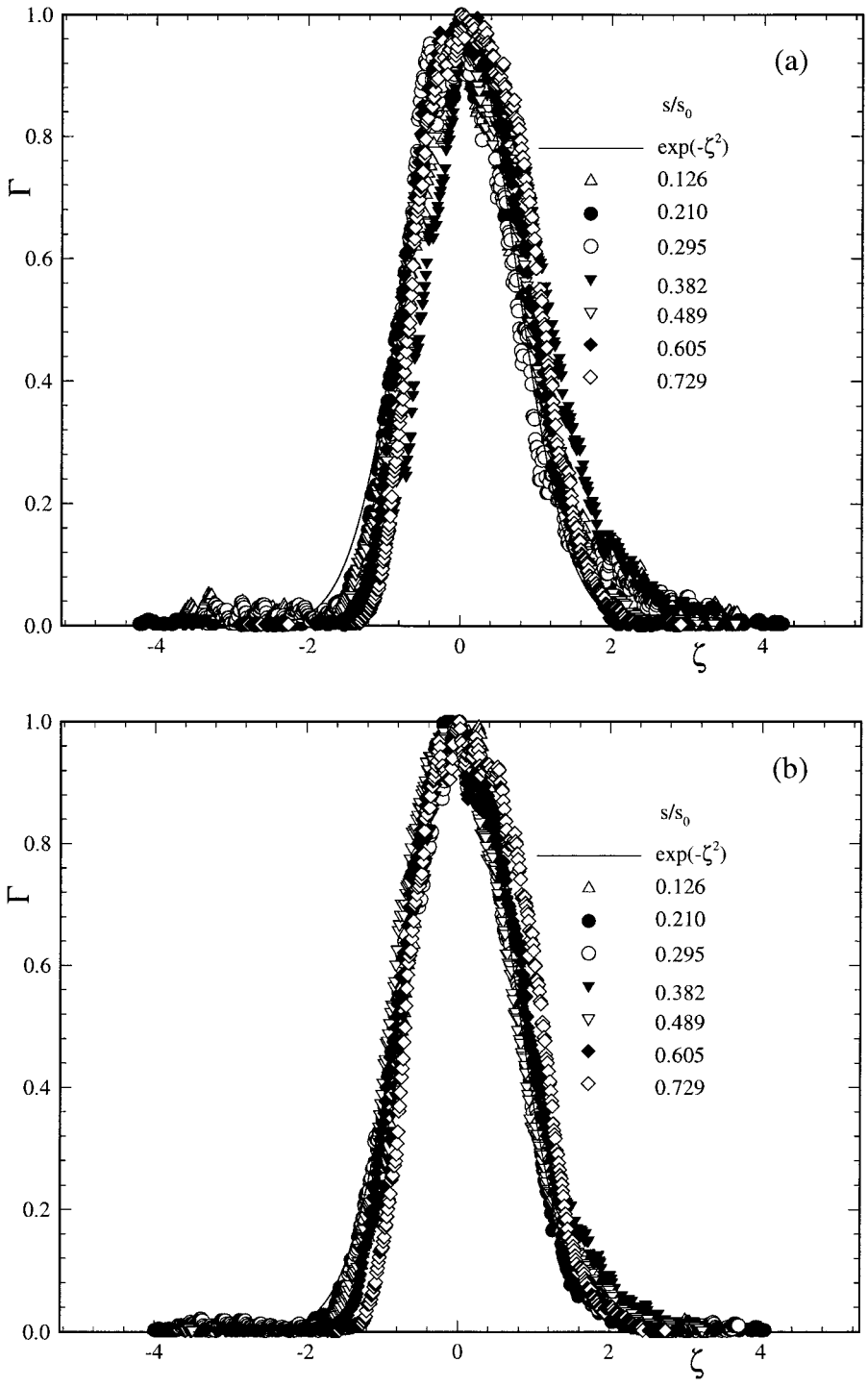


**FIGURE 14**
The relative intermittency as a function of nondimensionalized lateral coordinates. (a) $\Omega = 0.755$. (b) $\Omega = 1.51$ at $y = 0.1$ mm on the suction surface.

seemed to start at about $s/s_0 \approx 0.75$. As Figure 12 indicates, increasing the wake frequency, $\Omega$, from 0.775 to 1.51 by reducing the rod spacing resulted in an earlier transition start than occurred with rod spacing of 160 mm.

Two mechanisms are considered instrumental in affecting this transition start. The first is an earlier mixing of the wakes due to the reduction of their spacing, which leads to higher freestream turbulence that inherently affects the onset of the transition. The

second mechanism is the increased impinging frequency of the primary wake strips, which introduces an excessive turbulent kinetic energy transport to the boundary layer, causing a shift in the transition start toward the leading edge. It is conceivable that the combination of these two mechanisms would make additional contributions to the shift in the transition start. A further increase of $\Omega$ resulted in a higher freestream turbulence and increased impinging frequency and, thus, a significant shift in the transition toward the leading edge, as the consequence of the mechanisms discussed above. A similar turbulence intermittency pattern was observed for other y positions.

Figures 11 and 12 provide a qualitative insight into the complex intermittency picture in unsteady turbine cascade aerodynamics. Quantitative assessment of the intermittency is provided by the universal intermittency function presented in Figures 13 and 14 for the suction side and the pressure side, respectively. The relative intermittency function, $\Gamma$, is shown for the frequency values of $\Omega = 0.755$ and $\Omega = 1.51$ (160-mm and 80-mm spacings) on the pressure and suction surfaces, respectively, with the dimensionless longitudinal distance, $s/s_0$, as a parameter. Similar results were observed for other rod frequencies, as listed in Table 1 of Part I. The symbols represent the experimental data. For the reduced frequencies and longitudinal positions presented in these plots, the measured relative intermittency functions for wakes impinging on the blade surface closely followed Gaussian distribution, as given in Equation (1). A comparison of the relative intermittency results obtained from the turbine cascade with those obtained from the curved plate shows the universal character of this function. Using this function as a generally valid intermittency relationship for unsteady wake flows, the intermittency function $\langle \gamma_i(t_i) \rangle$ is determined completely by implementing Equations (2), (3), and (4) to discover additional information about the minimum and the maximum intermittency functions, $\langle \gamma_i(t_i) \rangle_{\min}$ and $\langle \gamma_i(t_i) \rangle_{\max}$.

### Heat-Transfer Coefficient Distribution

As indicated previously, a liquid crystal technique was used for the measurement of heat transfer because it does not affect the turbulence structure at the surface, as thermocouples or surface-mounted hot wire/film probes do. However, its slow response does not allow the extraction of valuable information about the unsteady state, so only time-averaged responses can be acquired in such cases. The heat-transfer coefficient distribution on the suction and pressure surfaces of the turbine blade for the four different wake-passing frequencies of $\Omega = 0$, 0.755, 1.51, and 3.02 are shown in Figure 15. These results confirm the investigations of the effects of unsteady flows on heat-transfer distribution in turbine blades by Han and colleagues (1993). The enhancement of the Stanton number by an increase in the wake-passing frequency is clearly apparent in these results. In the steady case on the suction surface, the transition starts near the trailing edge, and the beginning of the transition point moves toward the leading edge as the wake-passing frequency increases. Figure 16 shows the heat transfer distributions on the pressure and suction surfaces for $\Omega = 0.755$ and $\Omega = 1.51$. The three lines predict the heat-transfer coefficient corresponding to the maximum, minimum, and average intermittency functions plotted on these figures along with the experimental data shown by the symbols. The dashed curve represents the streamwise Stanton number distribution when the plate is subjected to an inlet flow intermittency state of $\langle \gamma(t) \rangle_{\max}$. The dot-and-dash curve depicts the Stanton number distribution when the blade is subjected to $\langle \gamma(t) \rangle_{\min}$. However, because of the periodic character of the inlet flow associated with unsteady wakes, the blade experiences a periodic change in heat transfer as an envelope. The liquid crystal responds to this periodic event with time-averaged signals, which are represented by the solid line. Figure 16 exhibits the Stanton number distributions along the suction surface for $\Omega = 0.755$ and $\Omega = 1.51$. Reasonably good agreement is seen for the entire laminar and transitional portions on the suction side of the turbine blade. Similar results were obtained for the pressure surface.

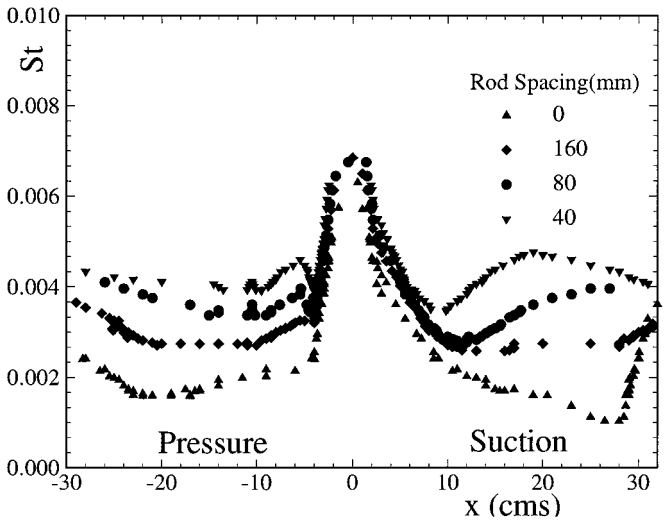


**FIGURE 15**
Stanton number distributions as a function of axial distance on the suction and pressure surfaces on the turbine blade for different rod spacings.

## CONCLUSIONS

This part of the article presents experimental verification of the unsteady boundary layer transition model discussed in Part I. The experimental data were obtained from a curved-plate and turbine-cascade unsteady research facility. Analysis of the data evidenced the universal character of the relative intermittency function developed in Part I. The transition model was implemented using an existing boundary layer code, and the results were compared with the measurement. The following conclusions were drawn.

1. The unsteady wake flow periodically changed the boundary layer transition from natural transition to wake-induced

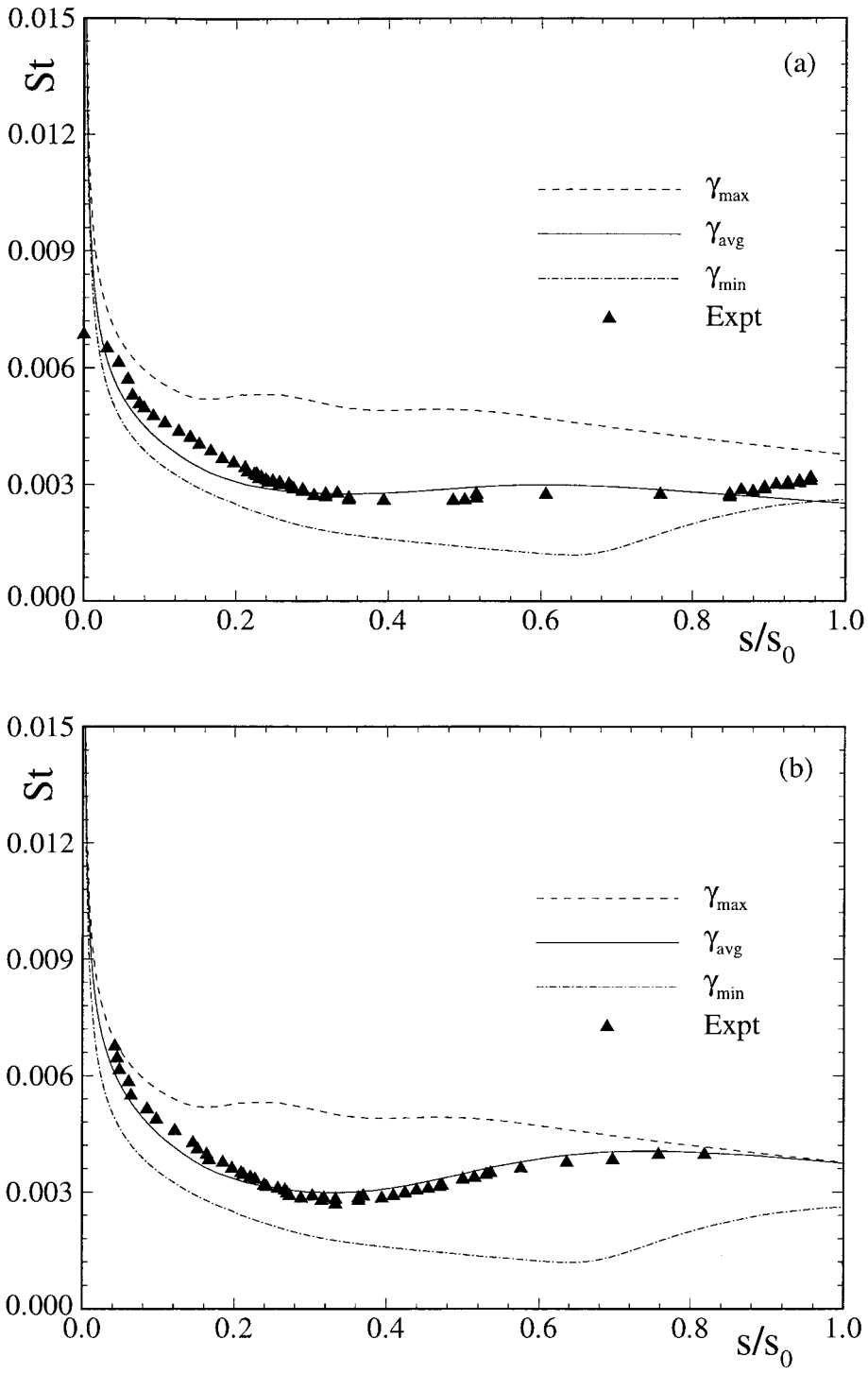


**FIGURE 16**
Stanton number distributions on the suction surface of the turbine blade as a function of axial distance. (a) $\Omega = 0.755$. (b) $\Omega = 1.51$.

transition, depending on the presence of a turbulent core inside the wake region.

2. The relative intermittency factor followed a Gaussian distribution. The minimum intermittency factor, $\langle \gamma_{min} \rangle$, represented the boundary layer behavior between the turbulent wake strips. It was shown to follow the natural transition process, as the freestream was almost nonturbulent. On the other hand, $\langle \gamma_{max} \rangle$, the value inside the turbulent core, started

with a value of $\approx$1.0 and went through a minimum. This was due to the viscous damping of the turbulent core by the boundary layer.

3. The transition model was implemented into a boundary layer code, which allowed for an accurate prediction of the aerodynamics and heat transfer along the curved plate and the turbine blade.
4. Based on these results, the implementation of the model into a Navier-Stokes code is expected to deliver results with high accuracy.

## REFERENCES

Han, J.-C., Zhang, L., and Ou, S. 1993. Influence of unsteady wake on heat-transfer coefficient from a gas turbine blade. *ASME Journal of Heat Transfer* 115:904–911.

Hippensteele, S. A., Russell, L. M., and Stepka, S. 1981. Evaluation of a method for heat-transfer measurements and thermal visualization using a composite of a heater element and liquid crystals. *ASME Journal of Heat Transfer* 105:184–189.

Mayle, R. E. 1991. The role of laminar-turbulent transition in gas turbine engines. *ASME Journal of Turbomachinery* 113:509–537.

Narasimha, R. 1957. On the distribution of intermittency in the transition region of a boundary layer. *J. Aero. Sci*. 24:711–712.

Pfeil, H., and Herbst, R. 1979. Transition procedure of instationary boundary layers. *Paper 79-GT-128*. American Society of Mechanical Engineers.

Schobeiri, M. T., Read, K., and Lewalle, J. 1995. Effect of unsteady wake-passing frequency on boundary layer transition: Experimental investigation and wavelet analysis. *Paper 95-GT-437*. American Society of Mechanical Engineers.